Species-Specific Long Range Interactions between Receptor/Ligand Pairs

R. Burchett Liebert and Dennis C. Prieve
Department of Chemical Engineering, Carnegie Mellon University, Pittsburgh, Pennsylvania 15213-3890 USA

ABSTRACT Total internal reflection microscopy (TIRM) monitors Brownian fluctuations in elevation as small as 1 nm by measuring the scattering of a single sphere illuminated by an evanescent wave when the sphere is levitated by colloidal forces such as electrostatic double-layer repulsion. From the Boltzmann distribution of elevations sampled by the sphere over time, the potential energy profile can be determined with a resolution of ~0.1 of the thermal energy kT. Thus, the interaction between a receptor-coated (goat, horse, or rabbit immunoglobulin G (IgG)) latex sphere and a protein A (SpA)-coated glass microscope slide was studied. A typical TIRM potential energy profile measured between a bare sphere and a bare glass plate, where the sphere fluctuates around the secondary potential energy minimum formed between double-layer repulsion and gravitational attraction, agrees well with DLVO theory. The interactions measured between IgG-coated spheres and SpA-coated slides, on the other hand, displayed a weaker repulsion compared with that observed between bare surfaces under the same conditions. Analysis of the results obtained between the coated surfaces suggests an additional attractive force. The decay length of this attraction correlates with the known dissociation constants for the binding of IgG with SpA in free solution.

INTRODUCTION

Most biological membranes contain receptor and/or ligand proteins that influence the specificity of cell adhesion. For example, an immune response is initiated when antigens interact with and bind to membrane-bound antibodies or antibody-like molecules of a lymphocyte. Also, leukocyte and tumor cell homing to particular tissues is accomplished by specific receptor interactions with endothelial ligands. Cell separation techniques, such as cell affinity chromatography (CAC), take advantage of specific receptor-ligand interactions to separate certain cells and detect target antibodies.

Several in vitro methods have been used to define the roles of nonspecific forces (such as van der Waals, electrostatic, and steric) and of specific receptor-ligand interactions in the adhesion process. Detachment assays, including centrifugation (Easty et al., 1960; McClay et al., 1981), hydrodynamic shear (Doroszewski, 1981; Forrester and Lackie, 1984; Weiss, 1961), and micromanipulation (Evans and Leung, 1984), are common techniques used to compare the ability of adherent cells to withstand a given force. Direct force measurements have been obtained recently using the atomic force microscope (AFM) (Florin et al., 1994) and the surface forces apparatus (SFA) (Leckband et al., 1992, 1994).

In this work, total internal reflection microscopy (TIRM) (Prieve et al., 1987, 1990) is used to measure the long range receptor/ligand interaction between a single receptor-coated polystyrene sphere and a complementary ligand-coated plate when the two surfaces are not in intimate contact. Measuring the interaction of a single Brownian particle offers advantages over the other direct force measurement techniques. Because it uses a molecular gauge (kT) for the energy rather than a mechanical gauge (spring constant) for the force, TIRM is capable of measuring much smaller interactions than either the SFA or the AFM. For example, forces as small as 10^{-13} N have been measured to within a few percent of known values with TIRM (Prieve and Frej, 1990), compared with 10^{-9} N with SFA (Parker and Claesson, 1992) or 10^{-11} N with AFM (Butt, 1991). This greater sensitivity allows TIRM to detect interactions at longer range, which may prove to be responsible for the "homing" of ligands toward receptors.

Specific receptor/ligand interactions are difficult to deconvolute from nonspecific forces that govern the binding of cells to surfaces. For this reason, we have chosen to use protein-coated 10-μm polystyrene spheres as model cells and protein-coated glass microscope slides as model surfaces. This model system has the advantage that nonspecific forces can be measured independently. Also, this model system is well suited for a TIRM study for the following reasons: 1) the high refractive index of the polystyrene spheres ($n_{sphere} \gg n_{cell}$); 2) the relative nondeformability of the spheres; 3) the covalent binding of the receptors to the spheres, thus immobilizing the receptor; and 4) the ability to vary the types and numbers of receptors.

Goat (g-), horse (h-), and rabbit (r-) immunoglobulin G (IgG) antibodies were chosen for the receptor to be linked to the carboxylate microsphere, whereas protein A (SpA) was chosen as the complementary ligand to be coupled to the glass microscope slide. SpA, a protein found in the cell wall of the *Staphylococcus aureus*, binds specifically to the Fc portion of immunoglobulins, IgG in particular, from various animal species. A control experiment will be performed to

Received for publication 8 July 1994 and in final form 3 April 1995.
Address reprint requests to Dr. Dennis C. Prieve, Department of Chemical Engineering, Carnegie Mellon University, Pittsburgh, PA 15213. Tel.: 412-268-2247; Fax: 412-268-7139; E-mail: prieve@cmu.edu.

0006-3495/95/07/66/08 $2.00

determine the amount of nonspecific attraction between coated surfaces by using SpA-deactivated IgG-coated microspheres.

In these experiments, the species of IgG coupled to the sphere was varied, thus altering the binding affinity between the receptor-coated sphere and ligand-coated surface. TIRM was then used to study the interaction between the model cell and surface. The experimental results were analyzed and compared with the measurements for uncoated surfaces.

TIRM

TIRM, first introduced by Prieve et al. (1987), monitors Brownian fluctuations in elevation as small as 1 nm by measuring the scattering of a single sphere illuminated by an evanescent wave when the sphere is levitated by colloidal forces (Fig. 1). Like the evanescent wave itself, the scattering intensity (I_{sca}) decays exponentially with separation distance (h) between the bottom surface of the sphere and the interface (Chew et al., 1979; Prieve and Walz, 1992):

$$I_{sca}(h) = I_{sca,o} \exp(-\beta h) \tag{1}$$

$$\beta = \frac{1}{n_2}\sqrt{(n_1 \sin\theta_1)^2 - n_2^2}, \tag{2}$$

where θ_1 is the incident angle (measured from the normal) of the beam forming the evanescent wave, $I_{sca,o}$ is the scattering intensity at $h = 0$ (sphere touching the plate), and n_1 and n_2 denote the refractive indices of the incident and transmitted media, respectively. β^{-1} is the characteristic decay length of the wave, frequently called the penetration depth. Under the conditions of the experiments performed, β^{-1} is on the order of 100 nm and a 1% change in scattering intensity corresponds to a 1-nm change in separation distance, which represents the spatial resolution of this technique. The sphere is held in a stable optical trap using a second laser beam (the radiation pressure beam) having a wavelength different from that producing the evanescent wave and focused along a vertical axis. This optical trap prevents Brownian motion tangent to the plate without restricting Brownian motion normal to the plate (Walz and Prieve, 1993).

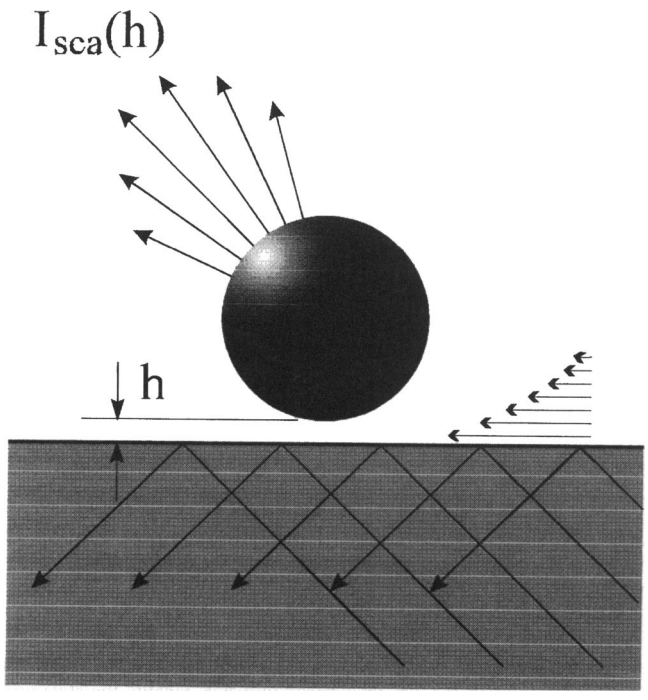

FIGURE 1 TIRM measures the intensity of light scattered by a single microscopic sphere illuminated by an evanescent wave (horizontal *arrows*). The scattered intensity $I(h)$ is exponentially sensitive to the elevation h.

Because the sphere undergoes Brownian motion, its instantaneous separation distance will fluctuate about an equilibrium position at which all of the forces are balanced (minimum potential energy). Let $p(h)\,dh$ denote the probability of finding the cell between h and $h + dh$, where h is the distance between the bottom of the particle and the glass slide. When observed over a sufficiently long time, the probability density $p(h)$ will be a Boltzmann distribution:

$$p(h) = A \exp\left(\frac{-\phi(h)}{kT}\right), \tag{3}$$

where $\phi(h)$ is the potential energy of the cell at elevation h, k is Boltzmann's constant, T is absolute temperature, and A is a normalization constant. From the Boltzmann distribution of elevations sampled by the sphere over a long time, the potential energy can be determined with a resolution of ~ 0.1 of the thermal energy kT.

Data are collected in the form of scattering intensity as a function of time. Typically 50,000 scattering intensity measurements are taken at 10-ms intervals and condensed into histograms. In the limit of a large number of observations, the shape of the histogram of intensities, $N(I_{sca})$, equals the shape of the probability density function for intensity, $P[I_{sca}(h)]$. However, Eq. 3 involves, instead, the probability density function for height, $p(h)$. Because the probability $p(h)\,dh$ of finding the particle between h and $h + dh$ is the same as the probability $P[I_{sca}(h)]\,dI_{sca}(h)$ of observing scattering intensity between $I_{sca}(h)$ and $I_{sca}(h) + dI_{sca}(h)$, the two probabilities are related. Scattering intensity is converted into elevation using Eq. 1, and the number of observations of any particular intensity is converted into potential energy (Prieve et al., 1987) using

$$\frac{\phi(h) - \phi(h_m)}{kT} = \ln\left[\frac{N[I_{sca}(h_m)]I_{sca}(h_m)}{N[I_{sca}(h)]I_{sca}(h)}\right], \tag{4}$$

where h_m is the most probable separation distance and $I_{sca}(h_m)$ and $N[I_{sca}(h_m)]$ are the scattering intensity and number of observations at h_m, respectively.

Expected potential energy profile

For the interaction of an uncoated sphere with an uncoated plate in a solution having an ionic strength $\leq \sim 1$ mol/m^3,

the potential energy profiles are found to be the sum of the double-layer repulsion (subscript dl) and gravitational (subscript gr) forces (Prieve et al., 1990).

$$\phi(h) = \phi_{dl}(h) + \phi_{gr}(h). \quad (5)$$

At higher ionic strengths, the particle also samples smaller separation distances for which van der Waals forces need to be considered.

For separations several times larger than the Debye length, the double-layer potential energy between a spherical particle and a flat plate can be calculated using linear superposition and the Derjaguin approximation, which is valid when $\kappa a \gg \kappa h \gg 1$ (i.e., a thin double layer) (Verwey and Overbeek, 1948). For a 1:1 electrolyte, this leads to

$$\phi_{dl}(h) = B\exp(-\kappa h). \quad (6)$$

$$B \equiv 16\epsilon a \left(\frac{kT}{e}\right)^2 \tanh\left(\frac{e\psi_1}{4kT}\right) \tanh\left(\frac{e\psi_2}{4kT}\right), \quad (7)$$

where a is the particle radius, e is the electronic charge, ϵ is the dielectric constant, and ψ_1 and ψ_2 are the Stern potentials of the particle and the plate. κ^{-1} is the Debye length defined by

$$\kappa = \left(\frac{e^2 \sum_i n_i^o z_i^2}{\epsilon kT}\right)^{1/2}, \quad (8)$$

where n_i^o and z_i are the bulk concentration and the valence of ion of type i, respectively.

The gravitational contribution for a sphere is

$$\phi_{gr}(h) = Gh, \quad (9)$$

where

$$G \equiv \frac{4}{3}\pi a^3(\rho_p - \rho_f)g - F_{rp} \quad (10)$$

is the apparent weight of the sphere, which equals the net buoyant weight (i.e., the actual weight less the weight of the displaced fluid), minus the upward force due to the radiation pressure, F_{rp}. Adding Eqs. 6 and 9 yields the total potential energy:

$$\phi(h) = B\exp(-\kappa h) + Gh. \quad (11)$$

This function has a minimum at a separation distance h_m given by

$$\kappa h_m = \ln\frac{\kappa B}{G}. \quad (12)$$

Eliminating B between Eqs. 11 and 12 gives

$$\frac{\phi(h) - \phi(h_m)}{kT} = \frac{G}{\kappa kT}\{\exp[-x] + x - 1\}, \quad (13)$$

where $x = \kappa(h - h_m)$ is the displacement from the most probable separation distance, expressed in Debye lengths.

In the absence of radiation pressure ($F_{rp} = 0$), the only two parameters that are needed to predict the shape of a potential energy profile are the values of the apparent weight G and the Debye parameter κ. G is computed from Eq. 10 and the known size and density of the polystyrene, whereas κ is calculated from (8) using the ionic strength inferred from independent measurements of the solution conductivity. Thus, the shape of the potential energy profile can be predicted with no adjustable parameters using Eq. 13. In this description, the charge parameter B does not affect the shape, but it does affect the location of the minimum, according to Eq. 12. Indeed, by observing the location of the minimum, we can infer the value of B that is related to the surface potentials ψ_1 and ψ_2 through Eq. 7. No other technique yields a direct measure of B or the surface potentials, although the zeta potentials can be measured and are often substituted for the surface potentials.

In the presence of an unknown amount of radiation pressure, the value of the parameter G must be determined by a regression of the linear portion of the potential energy profile. The difference between this value of G and the calculated net weight is the unknown radiation pressure force.

MATERIALS AND METHODS

Receptor and ligand

Rabbit, horse, and goat polyclonal IgG antibodies were used as the receptors on the beads. All of the antibodies were purchased in lyophilized powder form from Sigma Immunochemicals (St. Louis, MO) and used without further purification.

Recombinant SpA, prepared from the cytosol of an *Escherichia coli* strain containing the gene for SpA from *S. aureus* Cowan I strain, was chosen as the ligand. It was purchased from Zymed Laboratories in lyophilized powder form and used without further purification.

Glass slide preparation

Glass microscope slides (Fisher Scientific, Pittsburgh, PA) were cleaned vigorously by soaking in each of the following solutions for 20 min and subsequently rinsing with deionized water after each solution (note: all water used in the slide cleaning steps, protein coupling steps and TIRM experiments was filtered, double-deionized water): 1) 2% solution of hot Micro detergent (International Products Corporation, Burlington, NJ); 2) Chromerge cleaning solution (Fisher); and 3) 4 mM NaOH. After drying overnight at 100°C, the slides were treated with 3-aminopropyltriethoxysilane in acetone, forming an alkylamine carrier (Weetal, 1976) to which glutaraldehyde can couple. Glutaraldehyde, purchased as 8.0% in treated water from Eastman Chemical (Rochester, NY), was diluted to 1.1% v/v with water immediately before use. The slides were soaked in 5.0 ml of the glutaraldehyde solution for 2 h and then rinsed in water. This step converted the slide to an aldehyde carrier to which an amine group on the ligand was covalently coupled. Next, the slide was soaked in 5.0 ml of a 50 μg/ml SpA solution for 2 h, then rinsed in water. Finally, the slide was soaked for 2 h in glycine, to deactivate any remaining aldehyde groups on the glass surface, and again rinsed in water. The SpA-coated slides were stored at 4°C in storage buffer (PBS containing 0.1% sodium azide and 1.0% BSA) and were used within 2 days (Cozens-Roberts et al., 1990).

Polystyrene sphere preparation

Polystyrene latex microspheres were purchased as carboxylated microspheres, 2.5% suspension, from Polysciences, Inc. (Warrington, PA). They were reported to have an average diameter of 10 μm as determined by centrifuge assay. Carbodiimide chemistry, which covalently binds an amino group on the protein to an activated carboxylate group on the sphere (Polysciences, 1991), was used to couple the receptor to the bead surface. The chemicals and coating procedure were supplied in a carbodiimide coupling kit from Polysciences. The coating procedure involved preparation of the carboxylate surface by washing sequentially in carbonate and phosphate buffer solutions. A 2% solution of carbodiimide in phosphate buffer was added to the beads and mixed for 3–4 h. After the unreacted carbodiimide was removed by washes with borate buffer, 400 μg of the protein and 1.2 ml of borate buffer were added. The spheres were incubated with the IgG overnight and then washed in borate buffer to remove any uncoupled IgG. Ethanolamine was then added to block unreacted sites. The beads were stored at 4°C in storage solution and were used within 30 days.

The control beads (SpA-deactivated IgG-coated beads) were made by incubating IgG-coated beads overnight in a solution of 400 μg SpA in 1.2 ml of borate buffer. After incubation, the beads were washed in borate buffer to remove any uncoupled SpA. The SpA-deactivated IgG beads were also stored at 4°C in storage solution and were used within 30 days.

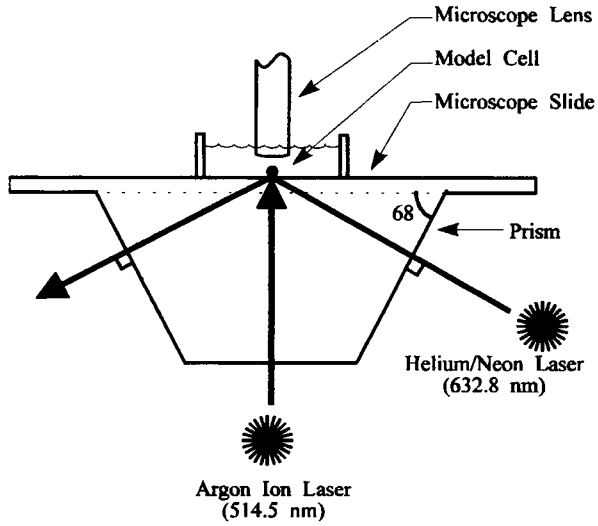

FIGURE 2 A simple schematic of the TIRM experimental apparatus. The Helium/Neon laser is used to create the evanescent wave, whereas the Argon Ion laser is used as the radiation pressure beam to hold and manipulate the particle.

Experimental procedure

Before beginning the experiment, the argon ion laser (Model 532–100A, Omnichrome, Chino, CA) and the computer were turned on to allow for normal warm-up. The helium-neon laser (Model 1137 P, Uniphase Corp., Manteca, CA) and the photomultiplier tube remained on continually to reduce evanescent wave drift and thermal noise, respectively.

Two NaCl solutions, one of low ionic strength (LIS) and one of high ionic strength (HIS), were prepared using deionized, ultra-filtered water (the water used throughout the experimental process). Typically, the LIS solution was 1 mM, whereas the HIS solution was 100 mM. Coated beads (50 μl) in storage solution were placed in a 1.5-ml centrifuge tube containing 1 ml of water and centrifuged for 2 min at 13,000 × g. The supernatant was discarded, and the tube was refilled with 1 ml of the LIS NaCl solution. The solution was centrifuged, and the supernatant was again discarded. These two centrifugation steps were performed to remove the storage buffer from the coated spheres. Again, 1 ml of the LIS NaCl solution was added to the tube, making a concentrated solution of coated spheres in low salt. Then, 4 drops from the centrifuge tube were added to 20 ml of the LIS solution. This diluted the concentration of coated spheres and produced the solution to be used in the experiment.

A schematic of the experimental setup is shown in Fig. 2. The 68° dovetail prism was cleaned with acetone and leveled with a spirit level. The helium-neon laser, used to produce the evanescent wave, was aligned by matching the back-reflection from the prism with the initial beam to ensure that normal incidence is attained. The argon ion laser, used to produce the radiation pressure, was aligned by swinging the focusing lens into place under the prism. A coated glass slide was removed from the storage buffer and rinsed well with water. The back of the slide was dried completely and then coupled to the prism via immersion oil. The experimental well was rinsed with the LIS solution without spheres and then filled with the diluted, coated-sphere solution. The 40× water emersion lens of a Zeiss Universal microscope equipped with a 10× eyepiece was then swung into place.

The experimental well, viewed through the objective, was positioned until a sphere was seen settling toward the surface. The radiation pressure beam was aligned under the settling particle using micrometer stages. The particle was then manipulated into the center of the microscope's field-of-view so that any scattered light could be detected by the photometry system, consisting of a Hamamatsu R-928 photomultiplier tube (PMT). A narrow bandpass filter (632.8 nm) was inserted above the objective to block extraneous light while permitting the scattered light to pass to the photomultiplier tube. The signal from the PMT was averaged electronically with a 30-μs time constant by the photometry system, and the analog output was fed to a Keithley 575 Measurement and Control Data Acquisition System that was coupled to a personal computer.

Scattering intensity measurements, typically 50,000 readings at 10-ms intervals, were taken at five or six radiation pressures. Next, the background intensity (scatter from dust in the solution or scratches and dust on the slide) was recorded by removing the particle from the photometry window using the radiation pressure beam. After the background intensity was recorded, the particle was returned to its previous position in the window.

Finally, the particle was "salted-out" (to reduce the double-layer repulsion) by adding 10 μl of the HIS salt solution to the experimental well to compress the double layer, causing the sphere to come in intimate contact with the plate. Again, scattering intensity measurements were taken and used as $I_{sca,o}$ in (1).

RESULTS AND DISCUSSION

Nonspecific interaction between uncoated surfaces

A typical potential energy profile (for the interaction between a bare 10-μm polystyrene sphere levitated above a bare glass microscope slide in a 0.5 mol/m^3 NaCl solution at a radiation pressure power of ~1 mW) is shown in Fig. 3. This profile has two distinct regions. At small separation distances, the interaction is dominated by the strong electrostatic repulsion and the potential decays exponentially with distance. At large separation distances, the sphere is outside the range of surface forces and experiences only gravitational and radiation-pressure forces. Because these latter forces are insensitive to location, the potential energy profile becomes linear in separation distance with a slope equal to the apparent weight (the net buoyant weight less the radiation pressure). The theoretical potential energy profile, calculated using Eq. 13 with G = 0.113 pN (chosen from the slope of the linear portion of the profile) and κ^{-1} = 14.2 nm (calculated independently from the measured solution

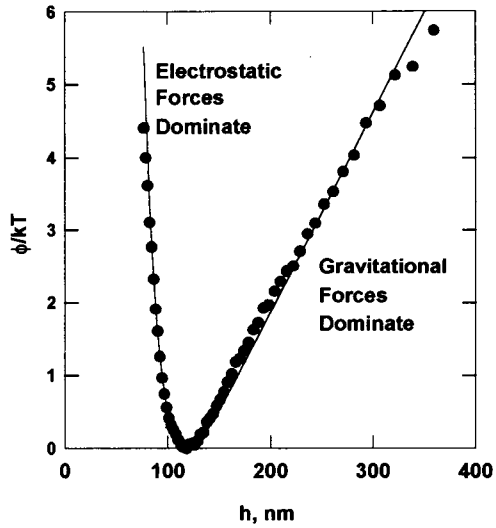

FIGURE 3 A typical potential energy profile measured with TIRM for a 10-μm polystyrene sphere above a glass slide in a 1.0 mol/m^3 NaCl solution. The theoretical line was calculated using Eq. 12.

conductivity) is also displayed in Fig. 3 for comparison. We have repeatedly obtained good agreement between the observed and expected profiles for interactions with uncoated spheres in solutions having ionic strengths of 1 mol/m^3 or less. At higher salt concentrations, the sphere resides closer to the plate and van der Waals attraction begins to become significant (Walz and Prieve, unpublished data).

Fig. 4 shows how the apparent weight depends on the power of the radiation pressure beam. Because the beam is pushing up on the particle, increasing the power decreases the apparent weight. By extrapolating to zero power, the actual net weight of the sphere was determined to be 0.199 $\pm$ 0.001 pN. Using a density difference of 0.055 $\pm$ 0.003 g/cm^3, this weight corresponds to a polystyrene sphere with a diameter of 8.90 $\pm$ 0.07 μm, which is well within the diameter range reported by the manufacturer (9.5 $\pm$ 0.9 μm).

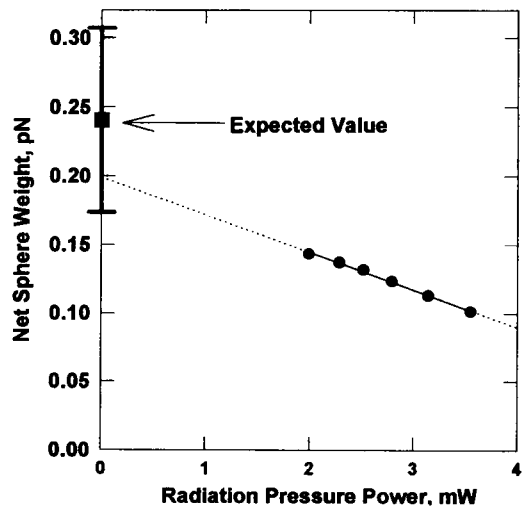

FIGURE 4 Net weight of a 10-μm polystyrene sphere as a function of radiation pressure power. The expected value is the weight calculated using a sphere diameter of 9.5 $\pm$ 0.9 μm and a density difference of 0.055 $\pm$ 0.003 g/cm^3.

Specific interaction between coated surfaces

In Fig. 5, the potential energy profile for a 10-μm r-IgG-coated polystyrene sphere in 1.0 mol/m^3 NaCl above a SpA-coated slide is shown along with the expected profile (Eq. 13) for an uncoated particle using G = 0.054 pN (chosen from the slope of the linear portion of the profile) and κ^{-1} = 10.3 nm (determined independently from the measured solution conductivity). Once again, when the apparent weight of the sphere (G) is determined as a function of radiation pressure and extrapolated to zero radiation pressure, a value is obtained for the actual net weight of the sphere that is well within the range expected for the range of sizes claimed by the manufacturer. However, comparison of the measured and expected profiles shows marked discrepancy on the left-hand side. In particular, the electrostatic repulsive portion of the experimental potential energy curve appears to be reduced compared with the repulsion predicted for an uncoated sphere.

The experimental profile does fit an equation of the form of (13) if the exponential decay length κ^{-1} is chosen to be larger than the Debye length. By subtracting the gravitational portion of the profile (ϕ_{gr}) from the measured experimental potential (ϕ) in Fig. 4, the contribution from colloidal forces is generated (Fig. 6 *a*). Assuming an exponential decay, the best-fitting line corresponds to an apparent decay length (κ_{app}^{-1}) of 16.4 nm. The curve produced when this exponential is recombined with the linear portion of the potential agrees much better with the exper-

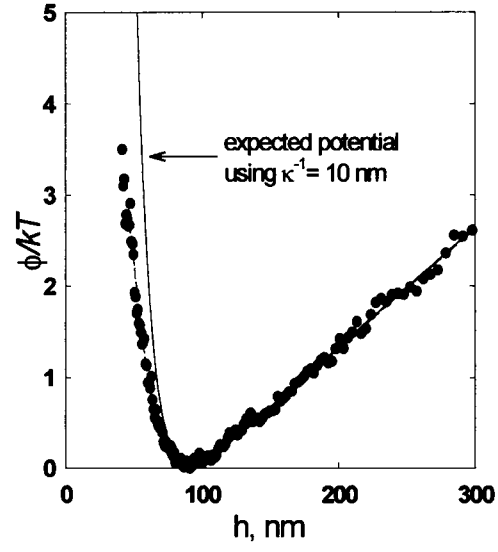

FIGURE 5 The measured potential energy profile (●) for a r-IgG-coated 10-μm polystyrene sphere interacting with a SpA-coated glass microscope slide in a 1.0 mol/m^3 NaCl solution. (——) The predicted potential for uncoated surfaces calculated using Eq. 13; (- - - -) the potential calculated using Eq. 14.

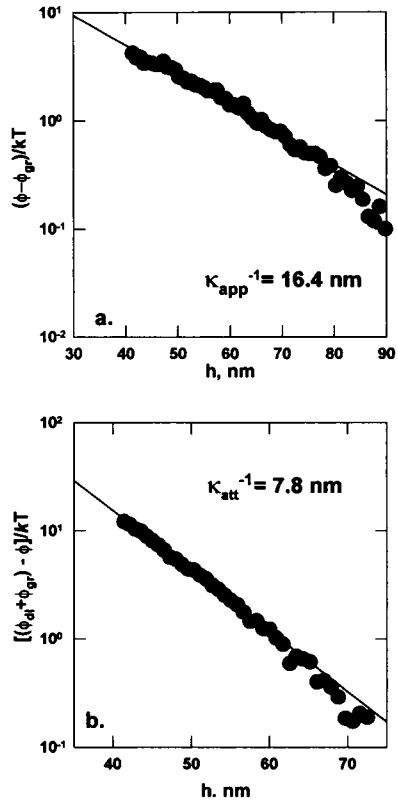

FIGURE 6 (*a*) By subtracting the gravitational contribution from the potential energy profile of Fig. 3, the colloidal contribution was obtained, which seems to decay exponentially with an effective decay length (κ_{app}^{-1}) of 16.4 nm. (*b*) The difference between the observed and the expected potential energy profile in Fig. 3 is an attractive potential that also decays exponentially with separation distance with an attractive decay length ($\kappa_{att}^{-1}\kappa$) of 7.8 nm.

imental profile than the predicted profile in Fig. 5 (in which the decay length is equal to the actual Debye length of 10 nm).

Is there any justification for using a decay length almost twice the Debye length? One possible reason is that the exponential decay of Eq. 13, in which κ^{-1} is the Debye length, was derived by assuming that the surface charges are confined to a plane of zero thickness. For the protein-coated surfaces used in this experiment, some of the surface charges come from amino acid residues that are distributed over the 5- to 10-nm thickness of the protein coatings on the sphere and on the plate. These coatings represent ion-penetrable layers whose interaction might be different from that of impenetrable surfaces. However, because these layers are thin compared with the most probable separation distance of 90 nm shown in Fig. 5, this difference may not be important. Ohshima and Kondo (1991) considered the effect of ion-penetrable layers and found that, until the layers overlap, the usual exponential decay applies with a decay length equal to the Debye length. When the layers overlap, the adjusted decay length turns out to be less than the Debye length. Thus, the correction for ion-penetrable layers is inconsistent with the longer decay length. Some other effect is suggested. Although a linear fit was applied to the results in Fig. 6 *a*, the data begin to curve slightly as the separation distance increases. This curvature suggests that the force or forces at work below the potential minimum are not a single-exponential function.

Instead of a modification to the electrostatic interaction, perhaps the deviation between the measured and the expected potential profiles represents an additional force that is specific to the r-IgG/SpA interaction. Subtracting the solid curve in Fig. 5 ($\phi_{dl} + \phi_{gr}$) from the measured one (ϕ) isolates this additional force, which has a negative (attractive) interaction energy and decays exponentially with separation distance (Fig. 6 *b*). The attractive decay length (κ_{att}^{-1}) associated with the regression line shown is 7.8 ± 0.22 nm. Equation 10 can be modified to account for this force with the addition of an attractive exponential term

$$\phi(h) = B\exp(-\kappa h) + Gh - C\exp(-\kappa_{att}h), \quad (14)$$

where C and κ_{att} are determined from Fig. 6 *b*, B is calculated from Eq. 12 and G and κ are already known. When Eq. 14 is plotted vs. h, the predicted potential now agrees with the experimental data over the entire range of separation distances.

Addition of the third term in Eq. 14 displaces the minimum toward smaller separations by about 1.6 nm compared with the minimum in Eq. 11. This displacement is well within the experimental uncertainty in determining the minimum in the experimental potential energy profile and was ignored when subtracting the solid curve from the experimental data to generate Fig. 6 *b*. To estimate the effect of this displacement, we shifted the solid curve 1.6 nm to the right; we also raised it by 0.021 kT to keep the linear portion coincident with that of the original curve. When this shifted curve is subtracted from the experimental data and the results regressed as in Fig. 6 *b*, the attractive decay length decreased by ~0.6 nm, which is a better measure of the uncertainty in the decay length than the SE produced by the regression analysis.

Nonspecific interaction between coated surfaces

To show that the attraction in Fig. 6 *b* is associated with the specific interaction between these two proteins, we deactivated the r-IgG that is attached to the sphere by saturating all of the binding sites with SpA before interacting the sphere with the SpA-coated microscope slide. The resulting experimental potential energy profile in 1.0 mol/m^3 NaCl is shown in Fig. 7 along with the predicted profile (Eq. 13) for an uncoated particle with κ^{-1} = 10.0 nm (calculated from solution conductivity). Note that the discrepancy between measured and expected profiles, which was so noticeable in Fig. 5, has virtually disappeared. This suggests that the attraction in Fig. 6 *b* is associated with the specific interaction between r-IgG and SpA.

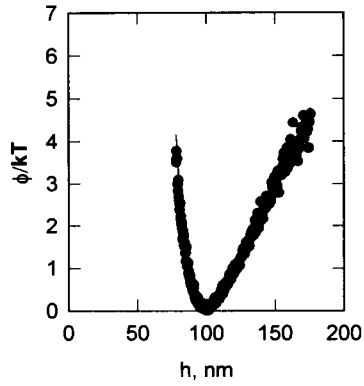

FIGURE 7 The measured potential energy profile (●) for a SpA-deactivated r-IgG-coated 10-μm polystyrene sphere interacting with a SpA-coated glass microscope slide in a 1.0 mol/m^3 NaCl solution. (——) The predicted potential for uncoated surfaces calculated using Eq. 13.

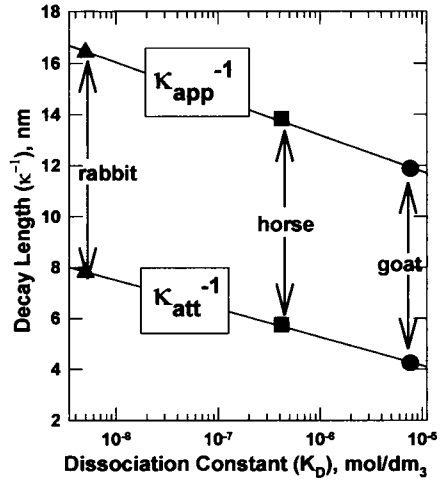

FIGURE 8 Experimentally determined apparent and attractive decay lengths plotted versus dissociation constant literature values for the binding of goat (Langone, 1982), horse (Goudswaard et al., 1978), and rabbit (Kessler, 1975) IgG to SpA in free solution.

Speculation on the origin of attraction

Leckband et al. (1992), using the SFA, studied the well characterized receptor-ligand system of streptavidin and biotin. They also reported a reduced repulsion that was attributed to a long range attraction between the streptavidin and biotin molecules (Leckband et al., 1994). The experimental attractive decay lengths for the interaction of streptavidin with a 5% biotin surface and a 0.5% biotin surface were determined to be 1.7 and 8.8 nm, respectively (Leckband et al., 1994). The attractive decay length reported here for the r-IgG/SpA system is similar to that found for the 0.5% biotin surface.

Although an attractive force between receptors and ligands is suggested, its origin remains uncertain. Leckband et al. attributed this attractive force to the "hydrophobic interaction between the exposed surfaces of the biotin and streptavidin binding sites" (Leckband et al., 1992). Perhaps the specific attraction between IgG and SpA has a similar origin. In support of this speculation, Deisenhoffer (1981) stated that the SpA forms predominately hydrophobic contacts with the IgG molecule. Many recent experiments (Israelachvili and Pashley, 1986; Claesson et al., 1982; Christenson and Cleasson, 1988) have observed strong long range attractive forces, between hydrophobized surfaces immersed in water, which also obey exponential decay.

Variation with species of IgG

Similar analyses leading to the attractive decay length were performed for the g-IgG- and h-IgG-coated particles interacting with SpA-coated microscope slides. Fig. 8 compares the experimentally determined apparent (κ_{app}^{-1}) and attractive (κ_{att}^{-1}) decay lengths for the goat, horse, and rabbit systems, with the corresponding dissociation constants (K_D) for the respective IgG/SpA binding in free solution. A correlation can be seen between the apparent or attractive decay length and the dissociation constant, the inverse of the bond affinity. The IgGs that show a stronger tendency to associate with SpA in free solution display a stronger attraction (longer range) in these experiments. This result is also consistent with by Kuo and Lauffenburger (1993), who found a similar correlation between the adhesion strength per receptor and the dissociation constant for the adhesion of IgG-coated polystyrene spheres to SpA-coated slides using the radial flow detachment assay. The fact that the attractive and adhesive forces can both be correlated with the dissociation constant suggests that there is some common basis for the long range attraction and adhesion of IgG to SpA. Because physical (rather than covalent) bonds are formed between receptors and ligands, it is possible that attraction and adhesion could have the same common basis.

Future plans are to apply radiation pressure to the top of the particle, thus pushing the sphere closer toward the surface, to study the effect of separation distance on this attractive force.

We thank the Keck Foundation and National Science Foundation for partial support of this work. We also thank Professor Douglas Lauffenburger for suggesting this study and Suzanne Kuo for helping with the initial preparations.

REFERENCES

Butt, H. 1991. Measuring electrostatic, van der Waals, and hydration forces in electrolyte solutions with an atomic force microscope. *Biophys. J.* 60:1438–1444.

Chew, H., D. S. Wang, and M. Kerker. 1979. Elastic scattering of evanescent electromagnetic waves. *Appl. Opt.* 18:2679–2687.

Christenson, H. K., and J. N. Claesson. 1988. Cavitation and the interaction between macroscopic hydrophobic surfaces. *Science.* 239:390–392.

Claesson, J. N., C. E. Blom, P. C. Herder, and B. W Ninham. 1982. Interactions between water-stable hydrophobic langmuir-blodgett monolayers on mica. *J. Colloid Interface Sci.* 114:234–242.

Cozens-Roberts, C., J. A. Quinn, and D. A. Lauffenburger. 1990. Receptor-mediated adhesion phenomena. *Biophys. J.* 58:107–125.

Deisenhofer, J. 1981. Crystallographic refinement and atomic models of a human Fc fragment and its complex with fragment B of protein A from *Staphylococcus aureus* at 2.9 and 2.8 Å resolution. *Biochemistry.* 22: 2361–2370.

Doroszewski, J. 1980. Short-term and incomplete cell-substrate adhesion. *In* Cell Adhesion and Motility. A. S. G. Curtis and J. D. Pitts, editors. Cambridge University Press, New York. 171–197.

Easty, G. C., D. M. Easty, and E. J. Ambrose. 1960. Studies of cellular adhesiveness. *Exp. Cell Res.* 19:539–548.

Evans, E., and A. Leung. 1984. Adhesivity and rigidity of erythrocyte membrane in relation to wheat germ agglutinin binding. *J. Cell Biol.* 98:1201–1208.

Florin, E. L., V. T. Moy, and H. E. Gaub. 1994. Adhesion forces between individual ligand-receptor pairs. *Science.* 264:415–417.

Forrester, J. V., and J. M. Lackie. 1984. Adhesion of neutrophil leukocytes under conditions of flow. *J. Cell Sci.* 70:93–110.

Goudswaard, J., J. A. Van Der Donk, A. Noordzij, R. H. Van Dam, and J.-P. Vaerman. 1978. Protein A reactivity of various mammalian immunoglobins. *Scand. J. Immunol.* 8:21–28.

Israelachvili, P. M., and R. M. Pashley. 1986. The hydrophobic interaction is long range, decaying exponentially with distance. *Nature.* 300: 341–342.

Kessler, S. W. 1975. Rapid isolation of antigens from cells with a staphylococcal protein A antibody adsorbent: parameters of the interaction of antibody-antigen complexes with protein A. *J. Immunol.* 115: 1617–1624.

Kuo, S., and D. A. Lauffenburger. 1993. Relationship between receptor/ligand binding affinity and adhesion strength. *Biophys. J.* 65:2191–2200.

Langone, J. J. 1982. Applications of immobilized protein A in immunochemical techniques. *J. Immunol. Methods* 55:277–296.

Leckband, D. E., J. N. Israelachvili, F.-J. Schmitt, and W. Knoll. 1992. Long-range attraction and molecular rearrangements in receptor-ligand interactions. *Science.* 255:1419–1421.

Leckband, D. E., F. J. Schmitt, J. N. Israelachvili, and W. Knoll. 1994. Direct force measurements of specific and nonspecific protein interactions. *Biochemistry.* 33:4611–4620.

McClay, D. R., G. M. Wessel, and R. B. Marchase. 1981. *Proc. Natl. Acad. Sci. USA.* 78:4975–4979.

McQuarrie, D. A. 1976. Statistical Mechanics. Harper & Row, New York.

Ohshima, H., and T. Kondo. 1991. On the electrophoretic mobility of biological cells. *J. Biophys. Chem.* 39:191–198.

Parker, J. L., and P. M. Claesson. 1992. Direct measurements of the attraction between solvophobic surfaces in ethylene glycol and mixtures with water. *Langmuir.* 8:757–759.

Prieve, D. C., S. G. Bike, and N. A. Frej. 1990. Brownian motion of a single microscopic sphere in a colloidal force field. *Faraday Disc. Chem. Soc.* 90:209–222.

Prieve, D. C., and N. A. Frej. 1990. Total internal reflection microscopy: a quantitative tool for the measurement of colloidal forces. *Langmuir.* 6:396–403.

Prieve, D. C., F. Luo, and F. Lanni. 1987. Brownian motion of a hydrosol particle in a colloidal force field. *Faraday Disc. Chem. Soc.* 83:297–307.

Prieve, D. C., and J. Y. Walz. 1992. Prediction and measurement of the optical trapping forces on a microscopic dielectric sphere. *Langmuir.* 8:3073–3082.

Polysciences, Inc. 1991. Carbodiimide Kit for Carboxylated Microparticles. Data Sheet #238F.

Verwey, E. J., and Overbeek, J. T. 1948. The Theory and Stability of Lyophobic Colloids. Elsevier, Amsterdam.

Walz, J. Y., and D. C. Prieve. 1993. Scattering of an evanescent surface wave by a microscopic dielectric sphere. *Appl. Opt.* 32:1629–1641.

Weetal, H. H. 1976. Covalent coupling methods for inorganic support materials. *Methods Enzmol.* 44:134–148.

Weiss, L. 1961. The measurement of cell adhesion. *Exp. Cell Res.* 8:141–153.